Comparison of Satellite Passive Microwave With Modeled Snow Water Equivalent Estimates in the Red River of the North Basin

Ronny Schroeder , Jennifer M. Jacobs , Eunsang Cho , Carrie M. Olheiser, Michael M. DeWeese,
Brian A. Connelly, Michael H. Cosh , *Senior Member, IEEE*, Xinhua Jia,
Carrie M. Vuyovich, and Samuel E. Tuttle

Abstract—The Red River of the North basin (RRB) is vulnerable to spring snowmelt flooding because of its flat terrain, low permeability soils, and the presence of river ice jams resulting from the river's northward flow direction. The onset and magnitude of major flood events in the RRB have been very difficult to forecast, in part due to limited field observations of snow water equivalent (SWE). Coarse-resolution (25-km) passive microwave observations from satellite instruments are well suited for the monitoring of SWE. Despite routine use in the Earth sciences community to document the impacts of climate change, the use of passive microwave observations in operational flood forecasting is rare. This paper compares daily satellite passive microwave SWE observations from special sensor microwave/imager (SSM/I) and special sensor microwave imager/sounder (SSMIS), advanced microwave scanning radiometer for earth observing system (AMSR-E), and advanced microwave scanning radiometer 2 (AMSR2) from 2003 to 2016 to modeled output from the SNOw Data Assimilation System (SNODAS) and Global Snow Monitoring for Climate Research -2 (GlobSnow-2) in the RRB to determine the differences between the remotely sensed SWE estimates and the model products currently used in flood forecasting. Results show statistically significant differences between the satellite observations and SNODAS in the northern region of the basin that were not evident in the southern region. Satellite estimates of peak SWE in the forecast subbasins in the northern region were 40–125% higher than the model results which points to the lack of ground observations used to constrain the model simulations. This paper recommends that satellite SWE observations should be considered for improving operational snowmelt forecasting in the RRB.

Index Terms—Advanced microwave scanning radiometer 2 (AMSR2), advanced microwave scanning radiometer for earth observing system (AMSR-E), flood forecasting, Global Snow Monitoring for Climate Research (GlobSnow), microwave, SNOw Data Assimilation System (SNODAS), snowmelt, snow water equivalent (SWE), special sensor microwave/imager (SSM/I).

I. Introduction

SNOW water equivalent (SWE) represents an important portion of the water cycle in the Northern Plains of the U.S. and is a critical element needed to improve snowmelt flood forecasts. In the Red River of the North basin (RRB), snowmelt runoff poses an annual risk of flooding which in 1997 caused a total of $4 billion in damages in the U.S. [1]. Snowmelt flood forecasting in the RRB currently relies on SWE information primarily from ground observations and airborne gamma radiation snow surveys [2]. Unfortunately, because there are not enough SWE observations to support operational hydrologic modeling in the RRB [3], forecasting errors can occur [4]. For example, the National Weather Service (NWS) North Central River Forecast Center (NCRFC) over-predicted peak snowmelt flow in the RRB by 70% in 2013 which prompted the construction of emergency levees at a cost to taxpayers of ∼$2 million.

The NCRFC considers *in-situ* SWE observations to be an accurate source of information. However, sparse SWE coverage and significant field-to-field variability exists among agricultural fields in the RRB which can make ground observations extremely unreliable at scales relevant to flood forecasting, unless multiple such observations representative of a hydrologic forecast basin are available. The NCRFC forecasters, therefore, consider airborne gamma radiation snow surveys that have footprint sizes large enough to account for small-scale variability (a fight line is approximately 16 km long and 300 m wide [2], [5]). Unfortunately, high costs associated with airborne surveys restrict measurements to about two times each winter season. Moreover, the reliability of airborne SWE measurements

R. Schroeder was with the University of New Hampshire, Durham, NH 03824 USA. He is now with the Applied Aviation Sciences Department, Embry-Riddle Aeronautical University, Prescott, AZ 86301 USA (e-mail: ronny.schroder@gmail.com).

J. M. Jacobs and E. Cho are with the University of New Hampshire, Durham, NH 03824 USA (e-mail: Jennifer.jacobs@unh.edu; ec1072@wildcats.unh.edu).

C. M. Olheiser is with the University Corporation for Atmospheric Research at the National Weather Service National Operational Hydrologic Remote Sensing Center, Office of Water Prediction, Chanhassen, MN 55317 USA (e-mail: olheiser@ucar.edu).

M. M. DeWeese and B. A. Connelly are with the NOAA/NWS/North Central River Forecast Center, Chanhassen, MN 55317 USA (e-mail: mike.deweese@noaa.gov; brian.connelly@noaa.gov).

M. H. Cosh is with the U.S. Department of Agriculture, Agricultural Research Service, Hydrology and Remote Sensing Laboratory, Beltsville, MD 20705 USA (e-mail: michael.cosh@ars.usda.gov).

X. Jia is with North Dakota State University, Fargo, ND 58108 USA (e-mail: xinhua.jia@ndsu.edu).

C. M. Vuyovich is with NASA Goddard Space Flight Center, Greenbelt, MD 20771 USA (e-mail: carrie.m.vuyovich@nasa.gov).

S. E. Tuttle is with Mount Holyoke College, South Hadley, MA 01075 USA (e-mail: stuttle@mtholyoke.edu).

Color versions of one or more of the figures in this paper are available online at http://ieeexplore.ieee.org.

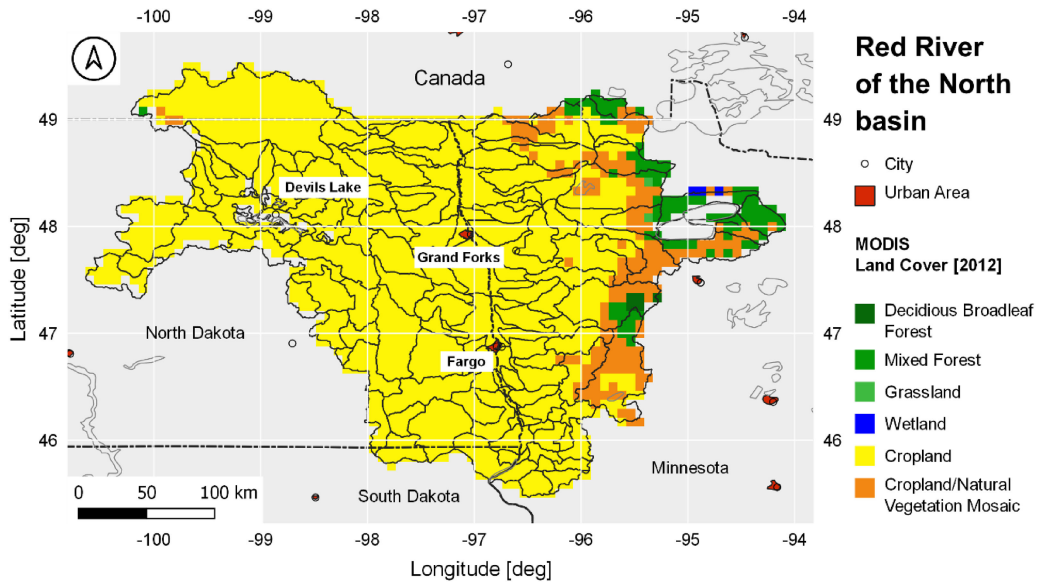Digital Object Identifier 10.1109/JSTARS.2019.2926058

Fig. 1. Red River of the North basin (RRB), its major cities and associated land cover as determined from the moderate resolution imaging spectroradiometer (MODIS) Collection 5 global land cover dataset, representing the year 2012. The North Central River Forecast Center (NCRFC) forecast subbasins are shown in black outlines.

depends on the accurate assessment of soil moisture conditions prior to an airborne survey [2], [5], [6].

Coarse resolution (∼25 km), near real-time, and satellite passive microwave SWE observations can provide flood forecasters with daily snow information anywhere in the RRB. The information can be provided day and night and independent of cloud cover, small-scale snow variability, or hazardous weather conditions. The detailed comparison of advanced microwave scanning radiometer for earth observing system (AMSR-E) satellite passive microwave SWE observations to airborne gamma radiation and ground snow survey SWE observations in the Northern Great Plains by Tuttle *et al.* [5] lends confidence to the value of satellite SWE observations in the RRB. The authors estimate a bias and RMSD of −3.8 and 34.7 mm between the satellite passive microwave SWE and ground observations.

Gridded model simulations of SWE from the National Oceanic and Atmospheric Administration (NOAA), National Weather Service's Office of Water Prediction (OWP) [formerly National Operational Hydrologic Remote Sensing Center (NOHRSC)], and SNOw Data Assimilation System (SNODAS) [7] can also support snowmelt flood forecasts because SNODAS SWE estimates are provided daily and cover the entire RRB. In SNODAS, numerical weather prediction output is used to force a physically based snow model that ingests ground-based, airborne, and satellite optical snow cover observations in near real-time. Although satellite passive microwave SWE observations have strong potential to support snowmelt forecasts [8], no previous studies have compared satellite passive microwave SWE observations to current operational model simulations of SWE for snowmelt forecasts in the RRB. Vuyovich *et al.* [9] identified the Northern Great Plains region as having significant differences between model and satellite SWE products.

This paper compares 13 years of daily satellite passive microwave SWE observations from special sensor microwave/ imager (SSM/I) and special sensor microwave imager/sounder

(SSMIS), AMSR-E, and advanced microwave scanning radiometer 2 (AMSR2) with model simulations from SNODAS and Global Snow Monitoring for Climate Research v2.0 (GlobSnow-2) in the RRB to identify differences among the datasets. We examine differences and provide a discussion about the datasets' potential value and limitations for snowmelt and flood forecasts in the RRB. The following sections will describe the study location, each of the SWE data sources, and the methods of comparison, followed by presentation and discussion of results.

II. STUDY LOCATION AND DATASETS

A. Study Area

The study region is the portion of the RRB for which the North Central River Forecast Center (NCRFC) provides river forecasts, which mostly lies within the U.S. (Fig. 1). The 101 500 km^2 forecast region comprises 147 individual NCRFC forecast basins. Basin delineations were obtained from the National Weather Service (NWS) Integrated Hydrologic Automated Basin Boundary System GIS database.[1] The Red River of the North forms the border between the states of North Dakota and Minnesota. It drains parts of eastern North Dakota, western central Minnesota, and a small area of northeastern South Dakota. Fargo and Grand Forks are the largest cities within the RRB and are located directly on the banks of the Red River (Fig. 1). The Red River flows northward, with the outlet of the RRB forecast region at the United States–Canada border. The land cover of the study area is predominantly cropland with mixed forest at the eastern edge of the basin (Fig. 1). The central Red River valley is extremely flat and the river elevation decreases only 40 m from Fargo to the Canadian border, or less than 20 cm per km [6]. This and the presence of snow during spring melt helps to explain why the

---

[1][Online]. Available: https://www.nohrsc.noaa.gov/gisdatasets/

basin is so vulnerable to snowmelt flooding. The region's climate is warm summer continental [10]. Winters are long and cold but lack the deep snow packs of the western Unites States due to the continental location of the basin and lack of orographic lift.

B. Datasets

This study compares SWE from operational passive microwave satellite observations and model output over a 13-year period (2003–2016). Each winter season is defined as a 34-week period starting on October 1st and ending in mid-May. The winter seasons are identified by water year (starting on October 1st). The corresponding winter season year is labeled by the end year. For example, the first winter in this study is 2004, and starts on October 1, 2003 and ends on May 25, 2004. For the satellite datasets, only night time (AMSR-E) and early morning (SSM/I) observations were used to minimize the effects of potential snowmelt events on the derived SWE values. Wet snow resulting from daytime heating erroneously lowers satellite passive microwave SWE estimates [11]. The temporal and spatial resolution of each dataset, origin, and corresponding retrieval algorithm or model simulation are described as follows.

1) AMSR-E and AMSR2: Daily, Level-3 AMSR-E SWE satellite observations in northern hemisphere equal-area scalable earth (EASE) grid format at 25-km spatial resolution were obtained from the National Snow and Ice Data Center (NSIDC) [12]. The AMSR-E SWE retrieval employs AMSR-E Level-2A swath brightness temperature (T_b) data [13] as input and the retrieval algorithm as outlined in Kelly *et al.* [14]. Daily, Level-3 AMSR2 SWE satellite observations were acquired from Japan's Aerospace Exploration Agency (JAXA) and are available for download through the Globe Portal System.[2] These data use the same retrieval algorithm as the AMSR-E product and are provided in equidistant cylindrical latitude-longitude grid format at a spatial resolution of 0.25°. The AMSR-E and AMSR2 retrieval algorithms use a set of T_b thresholds to detect the presence of wet and dry snow, as well as medium to deep or shallow snow, within the field of view [15]. Snow depth of the medium-deep snow is estimated dynamically for each pixel and separately for forested and nonforested pixel fractions. Scattering (i.e., the T_b difference between a low and high frequency band [16]) from snow in forested areas is detected using the 18-GHz vertical band as the baseline frequency. In forest-free regions, the longer wavelength 10-GHz vertical channel is used to increase the dynamic range and the detection of deep snow packs [15]. The resulting snow depths for each pixel fraction are combined and converted to SWE using the average *in situ* snow density [17], [18] found in the Sturm *et al.* [19], [20] snow classification map. The Level-3 dataset contains SWE data and quality flags. The data are available from June 19th, 2002 to October 3rd, 2011 and from July 2nd, 2012 to the present for the AMSR-E and AMSR2 datasets, respectively. Due to the same instruments and SWE estimation methods used, these two datasets are treated as one continuous record in this study.

2) SSM/I and SSMIS: Daily, Level-3 SSM/I and SSMIS satellite SWE was acquired from NSIDC. Inputs to the retrieval algorithm are T_b data, combining data from the SSM/I (F13)

and the more recent SSMIS (F17).[3] In this retrieval, SWE is derived using the Chang-based [16] NSIDC SWE algorithm of Armstrong and Brodzik [21] and an algorithm regression to extend the SWE record over multiple SSM/I and SSMIS satellite missions (M.J. Brodzik, NSIDC, personal communications). The combined SSM/I-SSMIS data provides SWE estimates from 2003 onwards. Data are provided in the Lambert azimuthal equal area projection at 25-km spatial resolution.

3) GlobSnow-2: The European Space Agency (ESA) provides daily, Level-3A GlobSnow-2 SWE model estimates, provided in northern hemisphere EASE grid format at 25 km spatial resolution. The most recent GlobSnow-2 snow model datasets contain long-term information on Northern hemisphere [35°–85°] SWE[4] (1979-2016). GlobSnow-2 SWE estimates derive from a data-assimilation scheme which combines satellite passive microwave radiometer observations with data from weather stations, as presented in Pulliainen [22] and Takala *et al.* [23]. Satellite inputs to the model include SMMR, SSM/I, and SSMIS T_b data in EASE grid format from the NSIDC. Weather station data are from the European Centre for Medium-Range Weather Forecasts (ECMWF). GlobSnow-2 SWE processing follows a four-step process—1) estimate snow depth (SND) over each EASE grid cell through an emission model inversion of the 18.7 and the 36.5 GHz passive microwave T_b bands calibrated to weather stations providing SND measurements, 2) convert estimated SND to estimated SWE using a snow density value for each grid cell, 3) generate an interpolated SND/SWE background map derived solely from weather station observations, and 4) construct the final SWE estimate [23], [24]. The last step uses a Bayesian spatial assimilation approach to combine data from 3) with the model estimates from 2). The underlying snow emission model of the GlobSnow-2 SWE data is the semiempirical HUT snow emission model of Pulliainen *et al.* [25]. The HUT snow model was previously validated against tower-based and airborne reference radiometer observations [25], [26]. The GlobSnow-2 SWE product also provides information on snow extent by using the SWE values as a means to describe overall snow extent [23]. Snow-free areas (0%), areas with melting snow (0%–100%), and areas with a full snow cover (100%) are denoted with 0, 0.001, and > 0.001 mm SWE, respectively. Melting snow is detected using the approach described in Takala *et al.* [27]. However, areas with periodic wet snow or a thin snow pack are not consistently identified and typically not contained in GlobSnow-2 [23]. Snow-free regions thus may include areas with occasional wet snow cover. Consequently, GlobSnow-2 SWE values are most reliable in regions with seasonal dry snow cover [24]. The data for this study are from the Version 2.0 dataset.[5] GlobeSnow is suitable for hydrological modeling and records are available in near-real time.[6]

4) SNODAS and Ground Observations: The SNODAS provides SWE model estimates for the contiguous U.S., in an equidistant cylindrical latitude–longitude grid at a grid spacing of 30-arc seconds ($\sim$1 km). SNODAS is an energy-and-mass balance snow modeling and data assimilation system that

---

[2][Online]. Available: https://gportal.jaxa.jp

[3][Online]. Available: http://cires1.colorado.edu/~brodzik/F13-F17swe/
[4][Online]. Available: http://www.globsnow.info/swe/
[5][Online]. Available: http://www.globsnow.info/swe/archive_v2.0/
[6][Online]. Available: http://www.globsnow.info/swe/archive_v2.0/

simulates SWE and other snowpack characteristics for the contiguous U.S. [28]. Model simulations of snow [3] are generated from hydrometeorological observations and downscaled gridded numerical weather model forcing using the mesoscale rapid update cycle (RUC2) prediction model [29]. The snow model employs the approaches by Tarboton and Luce [30] and Jordan [31] to solve for snow surface temperature energy and mass fluxes, respectively. Ground-based, airborne, and satellite optical snow cover observations from GOES and AVHRR are assimilated periodically using a Newtonian nudging technique to update the modeled snow states across the U.S. [28]. Annual counts of SWE ground and airborne observations assimilated into SNODAS in the RRB from 2003 to 2016 were used to support this study. The SNODAS data for this study are from the Version 1 data; masked (i.e., contiguous U.S.) data are available from September 30th, 2003 onwards [7].

III. METHODS

The four gridded daily SWE products, hereafter referred to as "SSM/I," "AMSR-E/2," "SNODAS," and "GlobSnow-2" are available for 12 water years, except in 2012 when no AMSR-E or AMSR2 data were available. To reduce the influence of wet snow contamination which tends to lower satellite passive microwave SWE estimates and ensure basin coverage for days with orbital gaps between satellite overpasses, weekly maximum SWE values were generated for each pixel for each gridded SWE product. Annual maxima for each water year were extracted from the weekly time series. Anomalous, very high SWE values (>300 mm) were observed in isolated AMSR-E and SSM/I pixels during early and late winter when SWE was generally low. SWE values that exceeded 300 mm during these periods were removed from the analysis. To facilitate comparison among the differently gridded SWE products, weekly and annual time series for each record period were spatially aggregated to the entire RRB, the northern RRB and the southern RRB (described in section 4.2), and the individual NCRFC forecast basins. Basins that contain large permanent water bodies are flagged within the SWE products. No assessment was made for these areas.

Significant differences in the population medians among annual and weekly SWE products were identified using the Kruskal–Wallis test [32] for each NCRFC forecast subbasin. The Kruskal–Wallis test is the nonparametric equivalent of the better-known analysis of variance (ANOVA). A significant difference indicates that at least one SWE product comes from a different population than the others but does not identify which products differ. The Dunn's test was conducted to identify which products differed only for basins for which the Kruskal–Wallis test identified significant differences ($p \leq 0.05$) [33]. To control the family-wise error rate of the Dunn's test, p-values for the testing of six sets of differences among the four SWE products were adjusted using the *Bonferroni* method [34]. The Kruskal–Wallis test was applied to annual maximum (or "peak") SWE as well as the weekly maximum SWE. The Dunn's test, when appropriate, was applied to the annual maxima.

Temporal correlation among the SWE products was examined by computing and comparing weekly climatologies and anomalies. The temporal analysis was stratified by NCRFC

forecast basin into northern and southern RRB following the results from the peak SWE Kruskal–Wallis test. The gridded weekly time series were used to construct weekly climatologies and corresponding weekly anomalies (i.e., with seasonality removed) for each SWE product, for both the northern and southern basin extent. The weekly climatology ($WClim$) was computed for each basin (i) and week (m) as follows:

$$WClim_{i,m} = \frac{\sum_{j=1}^{N} \text{SWE(Max)}_{i,m,j}}{N} \qquad (1)$$

where SWE(Max) is the weekly maximum gridded SWE averaged over each basin, j is the water year number, and N is the number of water years in the time series. A weekly anomaly time series was computed for each basin by subtracting the weekly climatology $WClim$ from the weekly time series of SWE(Max) for each SWE product and northern and southern basin extent i.

Relative differences (RelDiff) between the annual maximum SWE were computed by forecast subbasin for all SWE product combinations as follows:

$$\text{RelDiff}_i = \left[\frac{\sum_{j=1}^{N} \left(\text{SWE\_}A(\text{Peak})_j - \text{SWE\_}B(\text{Peak})_j \right)}{\sum_{j=1}^{N} \text{SWE\_}B(\text{Peak})_j} \right]$$
$$* 100 \qquad (2)$$

where SWE_A(Peak) and SWE_B(Peak) are the paired peak (i.e., annual maximum) SWE averaged over each NCRFC basin i (SSM/I & AMSR-E/2, SSM/I & SNODAS, SSM/I & GlobSnow, AMSR-E/2 & SNODAS, AMSR-E/2 & GlobSnow, SNODAS & GlobSnow).

IV. RESULTS

A. Differences Among the SWE Products

Fig. 2 shows the differences in peak SWE values among the four products from the Kruskal-Wallis test. Differences were detected among the four SWE products in much of the northern portions of the RRB. There are no significant differences among the SWE products in the southern RRB subbasins (Fig. 2). While not all forecast subbasins in the northern region are significantly different, there is a pattern of subbasins that exhibit consistently different behavior between the four datasets ($p \leq 0.1$).

The posthoc Dunn's test was conducted to identify which products are different from the others (Fig. 3). Clearly, the significant differences documented with the Kruskal–Wallis test in the northern forecast basins (Fig. 2) are due to differences between the satellite observations (SSM/I, ASMR-E/2) and the model outputs (SNODAS, GlobSnow-2). The test further indicates that these differences are primarily driven by differences between the satellite products and the SNODAS model. The satellite products and GlobSnow-2 differences are limited to the northwestern part of the basin. The satellite records only differ significantly in a single, remote basin in the far eastern portion of the RRB. Also, there are no significant differences between the SNODAS and the GlobSnow-2 products.

The Kruskal–Wallis test was also applied to the weekly SWE products (Fig. 4). Almost all the subbasins have significant differences early in the winter season (weeks 5–10). Those
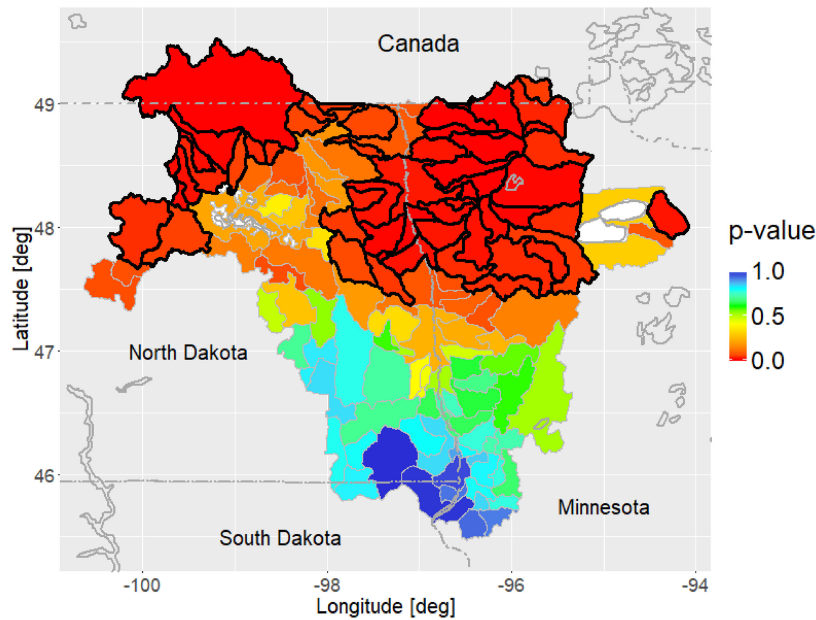
This article has been accepted for inclusion in a future issue of this journal. Content is final as presented, with the exception of pagination.

SCHROEDER *et al.*: COMPARISON OF SATELLITE PASSIVE MICROWAVE WITH MODELED SNOW WATER EQUIVALENT ESTIMATES 5

Fig. 2. p-values for the Kruskal–Wallis test for differences in annual maximum (SWE) from 2004 to 2016 for four operational SWE products (SSM/I, AMSR/E, AMSR2, SNODAS, and GlobSnow-2) in the RRB. Cold colors indicate weak evidence that the products differ and warm colors strong evidence. Forecast subbasins with significant differences of $p \leq 0.05$ are outlined in black. White areas contain large permanent water bodies (outlined in dark gray) and were excluded from the analysis. Smaller bodies of water (outlined in dark gray) are also visible in the RRB but were not excluded from the analysis. The forecast basins outlined in black and light gray correspond to the northern and southern RRB, respectively.
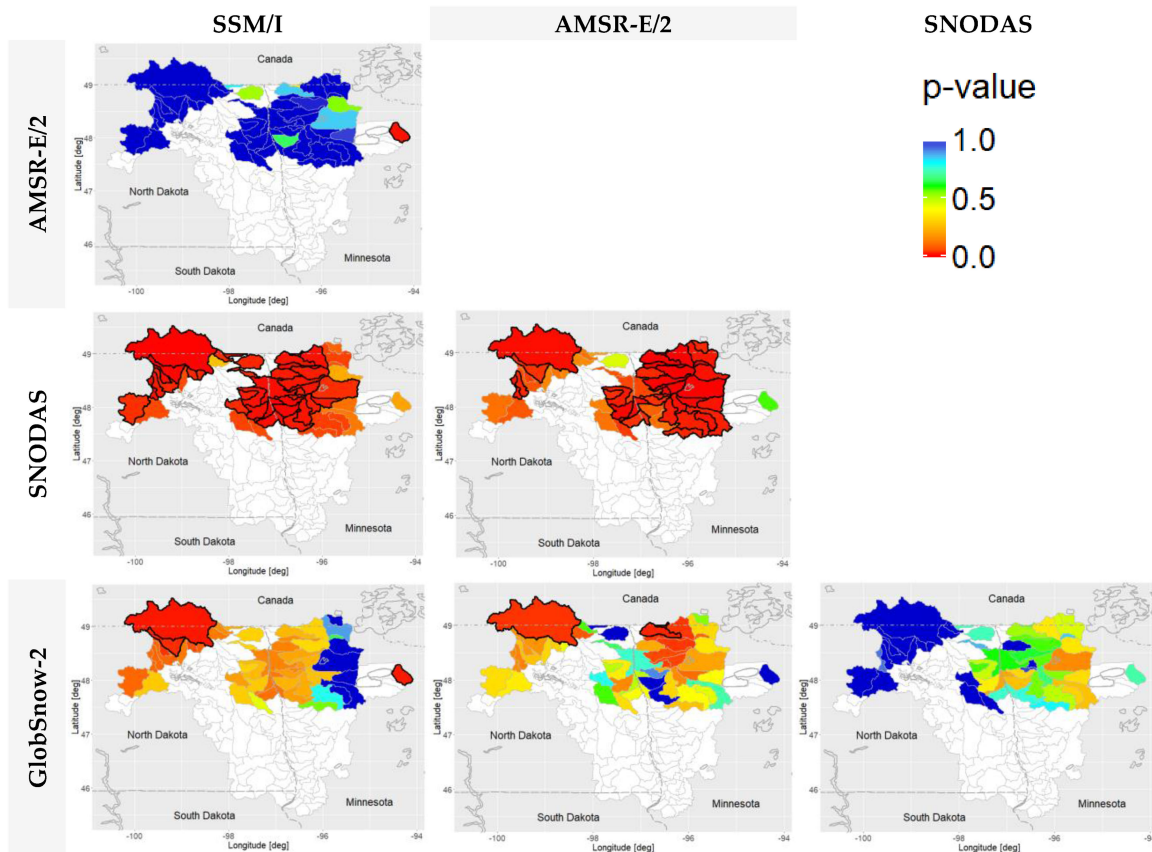

Fig. 3. p-value for the Dunn's test for differences in annual maximum SWE from 2004 to 2016 between the four operational SWE products (SSM/I, AMSR-E/2, SNODAS, and GlobSnow-2) in the RRB. Cold colors indicate weak evidence that the products differ and warm colors indicate strong evidence. Forecast subbasins with significant differences of $p \leq 0.05$ are outlined in black. White areas contain large permanent water bodies (outlined in dark gray) and were excluded from the analysis. White basins (outlined in light gray) are not significant as per the Kruskal–Wallis test and no Dunn's test was applied.
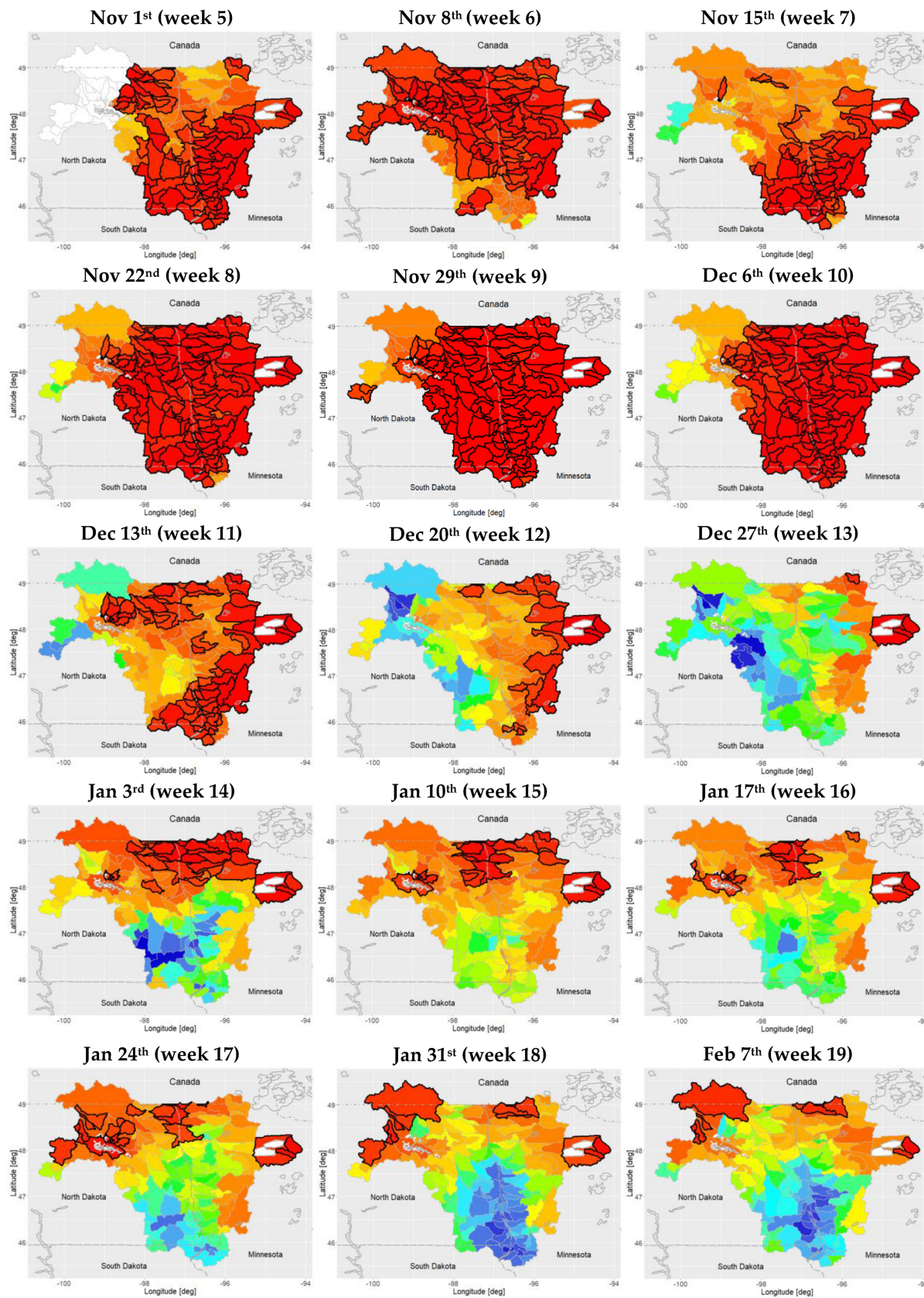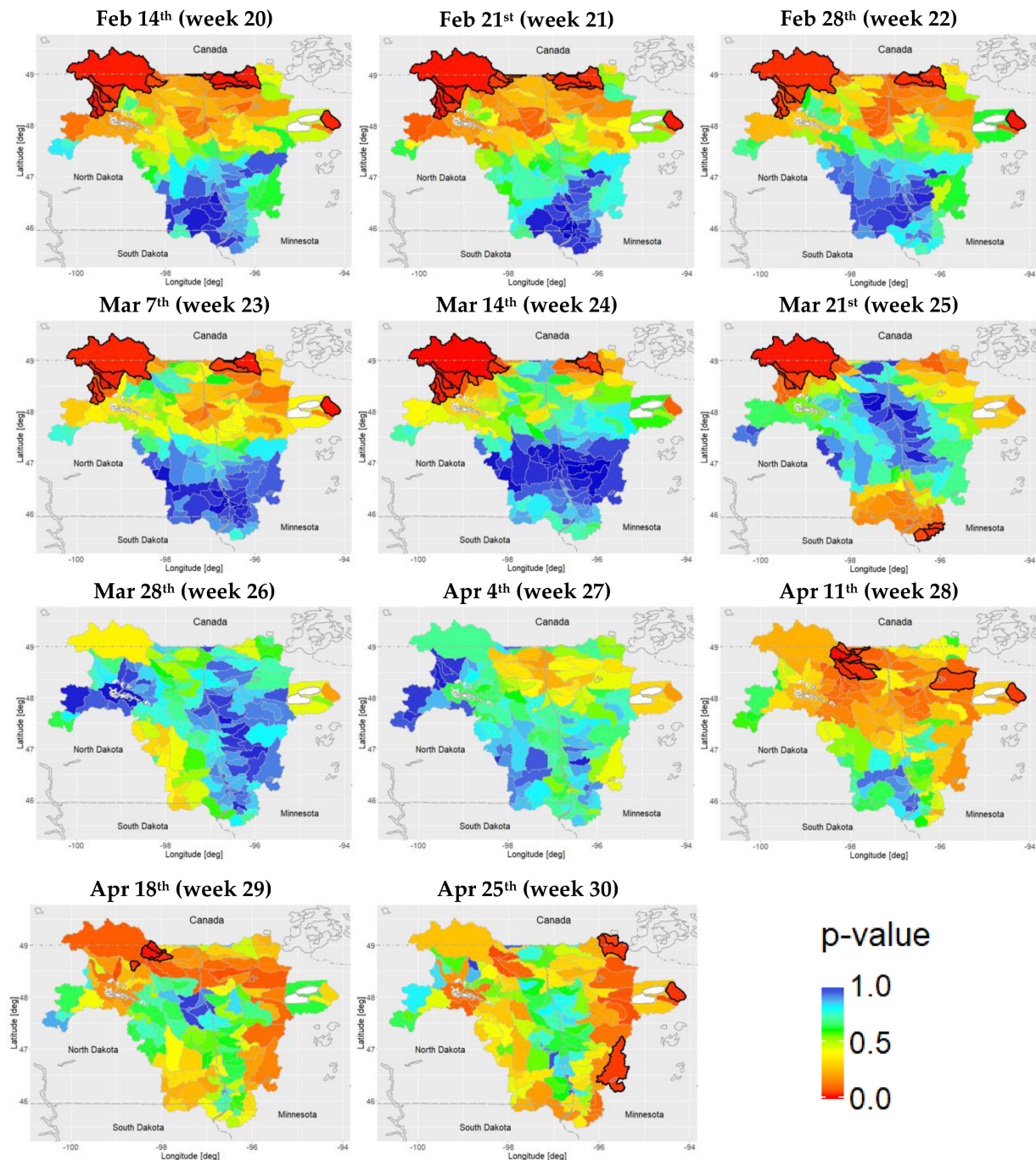
Fig. 4.   *(Contiuned.)*

Fig. 4. Same as Fig. 2 but for differences in weekly maximum SWE. Weeks 1–4 as well as week 31–34 are not shown due to data gaps in at least one of the SWE products.

differences almost entirely disappear by week 12 in December. However, in the northern RRB differences persist throughout much of the peak winter season (week 14–25), with many of the same basins identified in Fig. 2 identified here between week 14 and 25. However, there is no single week during the peak winter season where the patterns of significantly different subbasins match those shown in Fig. 2. This mismatch could suggest important differences in the timing of peak SWE among the products. Finally, the snowmelt season shows mixed results with virtually no differences among the SWE products early in the melt season (weeks 26–27). Dunn's testing of the differences in the northern RRB during the winter season are primarily driven by differences between the satellite products and the SNODAS model.

B. Relative Differences

Fig. 5 presents maps of pairwise relative differences of peak SWE among the four SWE products over the 12-year study period. There are virtually no differences in peak SWE between
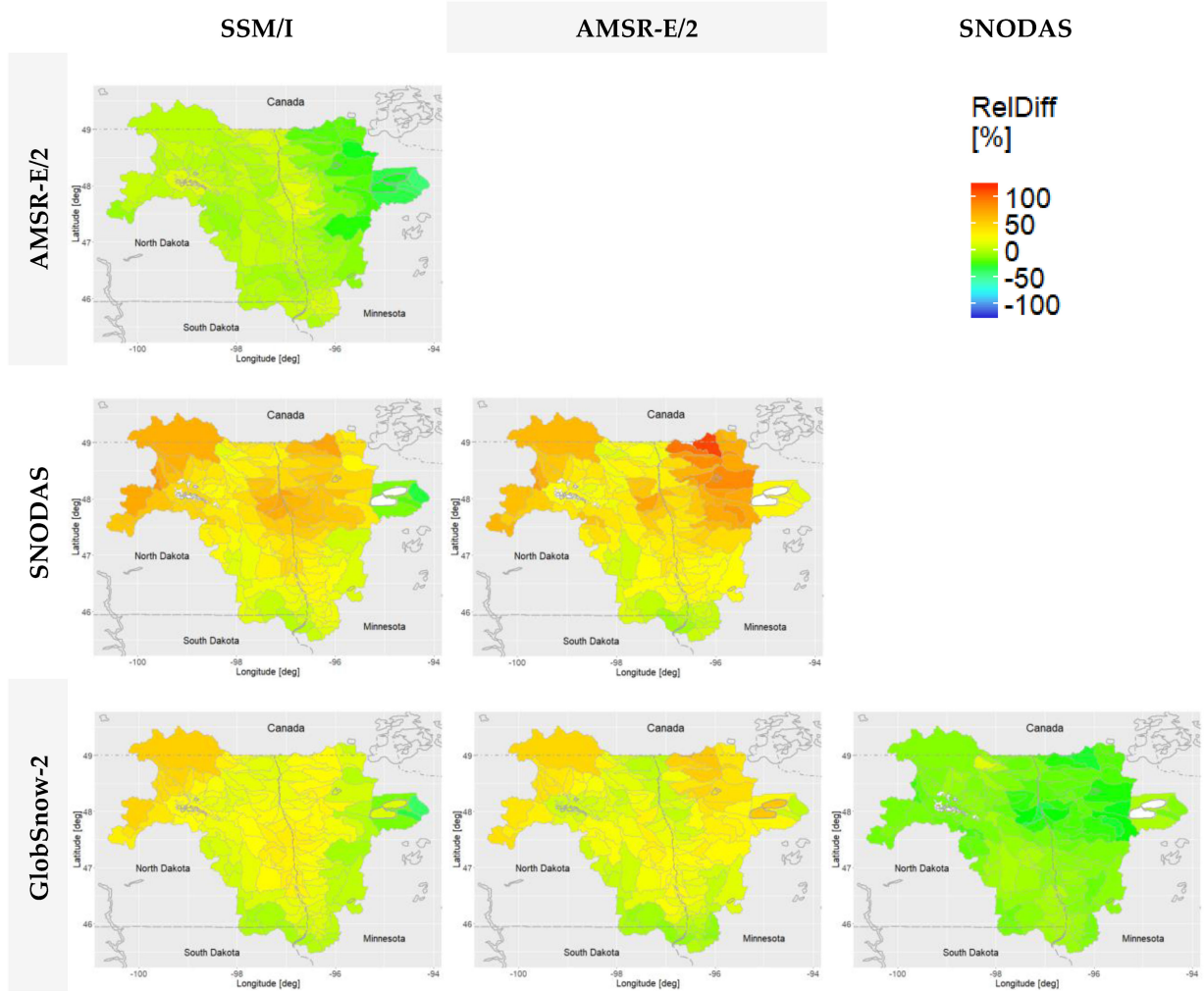
Fig. 5.   Relative difference in the RRB forecast subbasins from 12 years (2004–2016) of peak SWE using all combinations of the four operational SWE products (SSM/I, AMSR-E/2, SNODAS, and GlobSnow-2). Warm colors indicate a positive bias (product in the column has larger mean peak SWE than the product in the row) and cold colors a negative bias (column smaller than row). White areas represent large permanent water bodies (outlined in gray) and are excluded from the analyses against SNODAS.

the satellite products during the 12-year observation period, except in the northeastern corner of the basin where SSM/I is lower than AMSR-E/2 by approximately −25% (Fig. 5). The model results have small differences, 20–35 mm, with SNODAS tending to be lower than peak GlobSnow-2 SWE by approximately −25% particularly in the north-northeastern region (Fig. 5). The differences between the model and satellite peak SWE range from 20 to 100 mm (not shown). Basins that were significantly different in the posthoc Dunn's test have the largest absolute differences, with satellite peak SWE exceeding model peak SWE by 40–125% (Fig. 5). While the differences between GlobSnow-2 and the satellite SWE values are similar throughout the basin, greater differences are evident between SNODAS and the satellite products in some regions. For example, the center part of the basin near Grand Forks (Fig. 1) has high differences on the order of 40–90%, whereas the neighboring regions and the basins to the south show minor differences. Based on these results, the RRB was divided into the northern and southern basin for further analyses. The northern RRB includes all significantly different NCRFC forecast basins (outlined in black in Fig. 2) and the southern RRB contains the remaining forecast basins.

C. Temporal Agreement Among the SWE Products

The weekly climatology, annual time series, and the time series of anomalies from the climatology are shown in Figs. 6 and 7 for the northern and southern RRB, respectively. The northern portion of the RRB (Fig. 6) typically accumulates snow beginning in early November through the first week of March. The southern portion of the basin (Fig. 7) typically begins to accumulate snow a few weeks later. The snowpack declines relatively rapidly and disappears by early May. AMSR-E/2 has a relatively high SWE very early in the season. Peak SWE values are less than 100 mm, with the northern region's peak SWE exceeding that of the southern region by about 25 mm.

All products peak at about week 22, share similar melt period features, and have no snow by the 31st week. The greatest difference among the products is the magnitude of SWE during the peak snow season (weeks 18–23). There is a relatively large spread among the products in the northern basin's climatology [Fig. 6(a)]. This spread is much lower in the southern portion of the RRB [Fig. 7(a)]. In the north, SNODAS has the lowest average peak SWE (70 mm), AMSR-E/2 and GlobSnow-2 are nearly identical (82 mm), and SSM/I (95 mm) has the highest seasonal
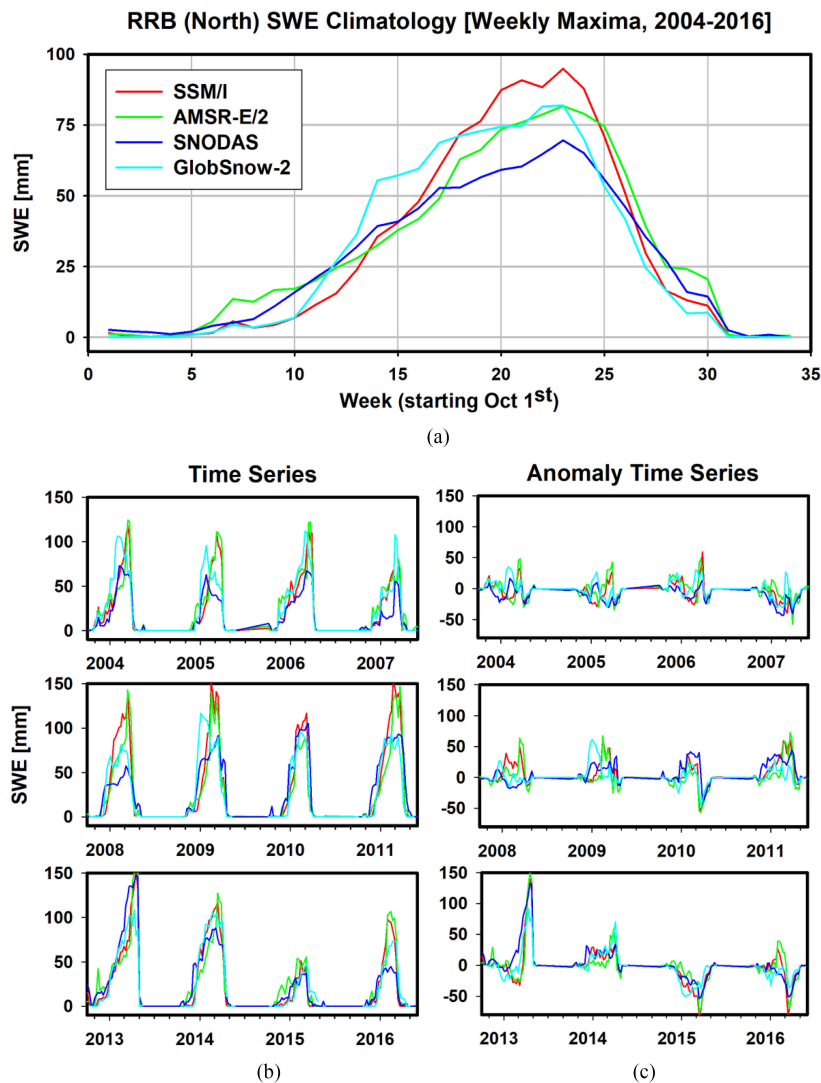
Fig. 6. Weekly SWE climatology (a), weekly time series (b), and weekly anomaly time series (c) from SSM/I, AMSR-E/2, SNODAS, and GlobSnow-2 SWE values from the northern RRB for 2004–2016. The weekly anomaly time series (c) is the weekly time series (b) minus the weekly SWE climatology (a). Time series values are spatial averages across all forecast subbasins where the Kruskal–Wallis test found a statistically significant difference between the SWE products (black outlines in Fig. 2).

peak SWE. In the south, SSM/I SWE is similar to GlobSnow-2 and only slightly higher than the other products. Differences are noted throughout the accumulation phase. SSM/I has greater SWE increases in the later part of the accumulation phase. GlobSnow-2 is nearly identical to SSM/I until week ten, then rapidly increases for several weeks, and remains higher than the other three products for much of the accumulation period.

The time series for the northern basin [Fig. 6(b)] shows that for all but three years (2010, 2013, and 2015) SNODAS has a considerably lower seasonal peak SWE, as much as 100%, relative to the satellite and GlobSnow-2 products. GlobSnow-2's patterns of snow accumulation and peak SWE are not consistent with the other products. In some years (e.g., 2007), GlobSnow-2 is greater than the other products, in other years, it tracks the satellite SWE closely, and in the remaining years, it is quite similar to SNODAS. In contrast, the differences between SNODAS and the satellite products are fairly consistent with SNODAS having lower SWE values in

most years. In a few years (e.g., 2010 and 2013), SNODAS is nearly identical to or exceeds the satellite products in the northern [Fig. 6(b)] and southern region [Fig. 7(b)], respectively.

Despite the differences in magnitude, the weekly SWE anomalies in Figs. 6(c) and 7(c) show that all the SWE products typically agree on which periods have relatively more and less snow when compared to the products' weekly climatology. For example, there is good agreement in the sign and evolution of SWE anomalies among the products in 2013 (a large positive SWE anomaly) and 2015 (a large negative SWE anomaly) in both the northern [Fig. 6(c)] and southern [Fig. 7(c)] RRB. The anomaly signals are clearest in years with much higher than average SWE values or less SWE. Moderately higher values in SWE are more difficult to discern. For example, in 2008, a consistent signal is not evident throughout the basin. Similarly, in the northern basin, the model and satellite products disagreed about the timing of peak SWE, e.g., in 2005 [Fig. 6(b) and (c)], which supports earlier findings (Fig 4).

This article has been accepted for inclusion in a future issue of this journal. Content is final as presented, with the exception of pagination.

10   IEEE JOURNAL OF SELECTED TOPICS IN APPLIED EARTH OBSERVATIONS AND REMOTE SENSING
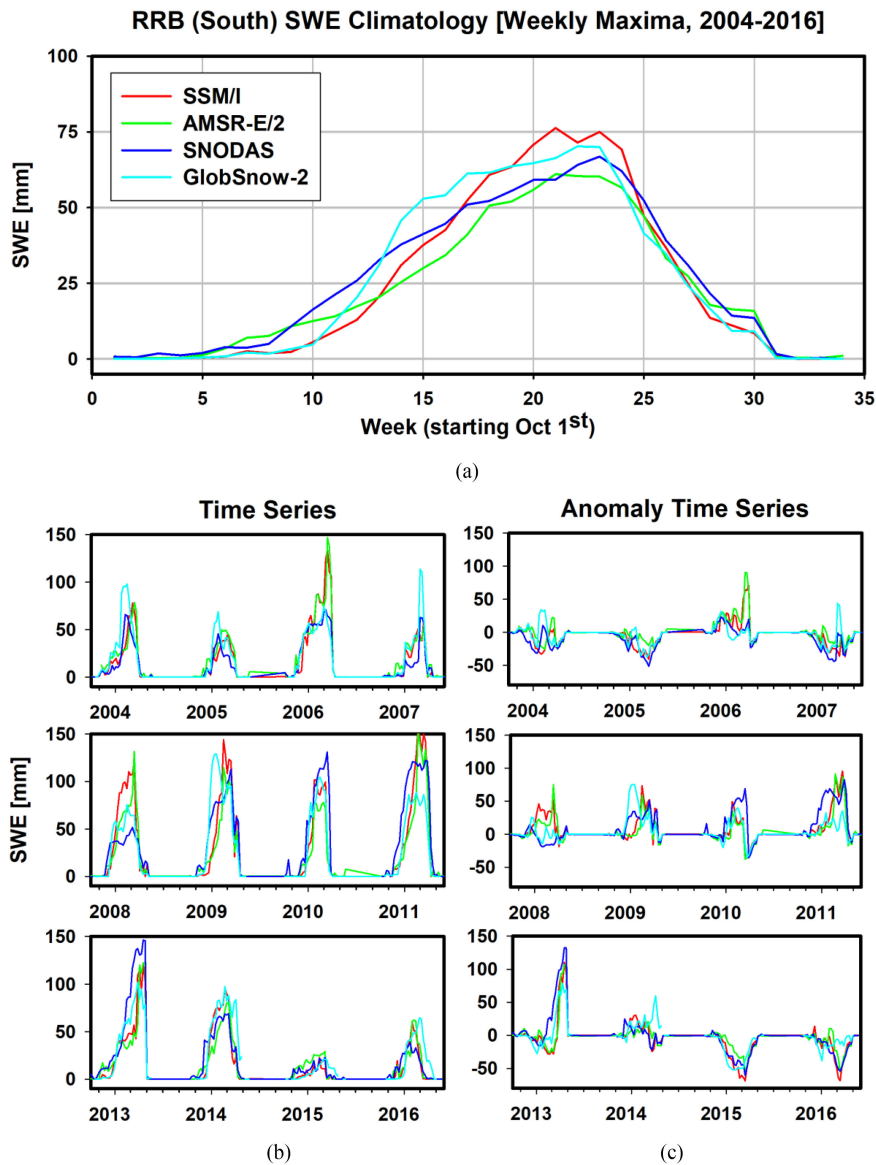

Fig. 7. Same as Fig. 6 but for the southern RRB. Time series values are spatial averages across all forecast subbasins where the Kruskal–Wallis test did not find a statistically significant difference between the SWE products (light gray outlines in Fig. 2).

The strength of temporal correspondence between the SWE products can be summarized by their temporal correlation on a weekly basis. Fig. 8 presents pairwise correlations between the SWE products determined from the weekly anomaly time series [Figs. 6(c) and 7(c)]. The satellite products are strongly correlated with one another (R ~ 0.9, p < 0.01). The overall correspondence between the satellite and model products is lower but still significant (R 0.5-0.7, p < 0.01). The satellite products show better agreement with SNODAS than with GlobSnow-2. SSM/I SWE agrees better with the model simulations than AMSR-E/2 SWE.

V. DISCUSSION

Previous research identified differences between model and satellite SWE products in the Northern Great Plains region [9]. In the current study, the peak SWE product comparison identifies highly localized differences between the satellite observations and SNODAS in the northern RRB that were not present in the southern region. Satellite estimates of peak SWE in the forecast subbasins in the northern region were 40–125% higher than the model results. This region is notable for its extremely sparse *in situ* data available to update the SNODAS simulation. Indeed, 15 or fewer *in-situ* or airborne SWE observations were assimilated into SNODAS in the northern region during the 13-year study period (Fig. 9). The region is also noted for having poor radar precipitation coverage [35]. This lack of ground observations in the northern region was also noted by Vuyovich *et al.* [9] and Josberger *et al.* [36] who conclude that satellite passive microwave SWE observations can enhance snowpack information in the northern Great Plains region. From Fig. 9 it appears that good agreement between model and satellite estimates generally corresponds to where the most *in-situ* observations are available. Exceptions to this pattern are the southwestern (northeastern) portion of the basin where a relatively low (high) number of observations exist. Relative differences between the satellite and

This article has been accepted for inclusion in a future issue of this journal. Content is final as presented, with the exception of pagination.

SCHROEDER *et al.*: COMPARISON OF SATELLITE PASSIVE MICROWAVE WITH MODELED SNOW WATER EQUIVALENT ESTIMATES 11
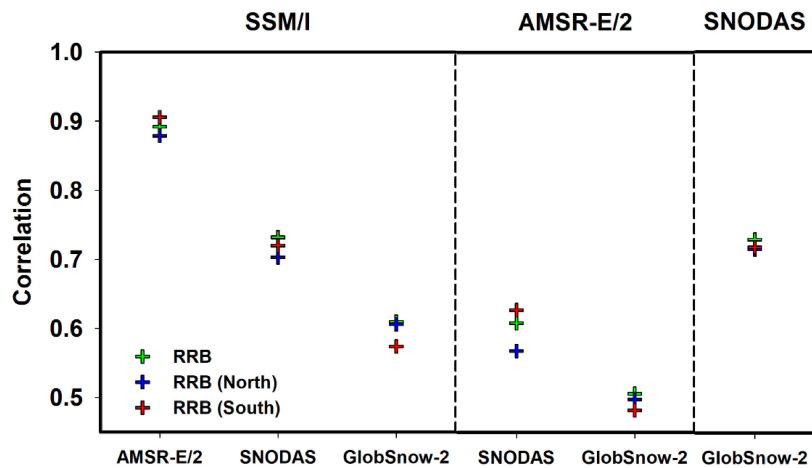

Fig. 8. Correlation values between weekly maximum anomaly SWE values from SSM/I, AMSR-E/2, SNODAS, and GlobSnow-2; in the northern, southern, and entire RRB for 2004–2016. All relationships are statistically significant at a significance level of 0.01.
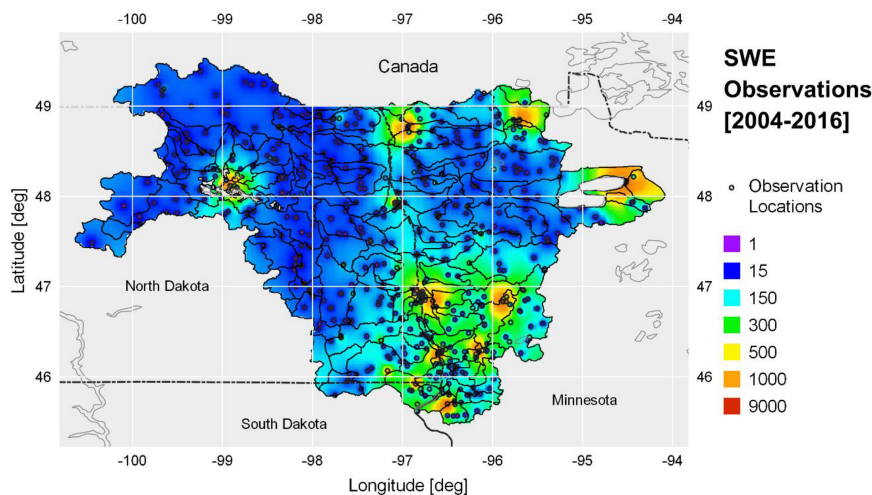

Fig. 9. Total number of SWE observations in the RRB for the period 2004–2016. Circles indicate locations of NOAA airborne gamma flight lines and ground stations. The number of observations collected at each location is shown by the circle color. Point locations were interpolated using inverse distance weighted interpolation to help visualize the number of observations used to support SNODAS in different parts of the RRB. Actual figure color is a linear interpolation of the colors in the legend.

model estimates in the northern region were less pronounced for the comparison against the GlobSnow-2 estimate which was not surprising because the GlobSnow-2, in addition to ground observations from the region, assimilates satellite passive microwave T_b data [22], [23].

No peak SWE differences were detected between the two model estimates, likely because both models are constrained by ground observations. There was only one RRB subbasin that showed a significant difference between the two satellite estimates of peak SWE. This difference can be explained by that subbasin's dense forest canopy [6], [36]. Unlike the SSM/I SWE retrieval algorithm [21], the AMSR-E/2 SWE retrieval algorithm explicitly accounts for the effects of forest cover on SWE [9], [14], [15], [37]. Overall, both SSM/I and AMSR-E/2 can provide a consistent record of peak SWE for similar regions with shallow snowpacks and limited dense forests [38].

The satellite estimates showed better temporal correlation with SNODAS than GlobSnow-2. This result was somewhat

surprising because SNODAS does not assimilate passive microwave satellite data for estimating model SWE whereas the GlobSnow-2 does. The lower temporal correspondence for the GlobSnow-2 may be attributed to differences in the snowmelt detection approaches and the general poor performance of GlobSnow-2 with thin snowpacks and periodic wet snow conditions [23] which are not uncommon in the RRB [5], [6].

Relatively poor temporal agreement between the satellite and model estimates may, in part, be caused by the updates made to the SNODAS [3], [28] and GlobSnow-2 SWE [22], [23] using ground observations which do not occur on a regular schedule nor cover the entire basin as compared to the twice-daily satellite observations. The SSM/I SWE showed better temporal correlation with model estimates than the AMSR-E/2 implying that SSM/I SWE might be more useful for real-time flood forecasting than the AMSR-E/2 in the RRB and similar regions. It seems reasonable that the lower temporal correspondence of the AMSR-E/2 stems from differences between the SWE retrieval

This article has been accepted for inclusion in a future issue of this journal. Content is final as presented, with the exception of pagination.

12   IEEE JOURNAL OF SELECTED TOPICS IN APPLIED EARTH OBSERVATIONS AND REMOTE SENSING

algorithms, the frequency bands employed, and the utility of T_b thresholds for wet snow detection that might not be optimal for use in the RRB. Forest cover [37], [39], wet snow [40], water vapor and cloud cover [41]–[43], and unintended penetration into underlying (wet) soil layers [44], [45] using lower frequency T_b observations (e.g., 10 GHz) in the AMSR-E/2 SWE algorithm can bias satellite SWE estimates. The satellite SWE estimates are also expected to be poor in the presence of water bodies [46], lake ice [47], ground ice, ice lenses [48], and depth hoar, all of which offer characteristically different T_b signatures that vary with frequency [26].

VI. CONCLUSION

Model simulations of SWE from SNODAS and GlobSnow-2 provide a potentially useful dataset of basin-wide SWE estimates in the RRB. However, accurate model estimates of SWE are largely dependent on accurate precipitation forcings and sufficient ground measurements to constrain model estimates. Unfortunately, high-quality *in-situ* observations of SWE are sparse in the RRB, particularly prior to maximum accumulation, and radar coverage is poor. Accurate determination of SWE for operational flood forecasting purposes therefore remains challenging. Satellite passive microwave SWE observations have the potential to overcome this challenge by providing flood forecasters with up-to-date, independent SWE information across the entire RRB.

While there are no significant differences between the peak SWE products across the southern RRB, the satellite passive microwave SWE estimates differ significantly from the model estimates across the northern domain of the RRB. The weekly time series show that differences occur throughout the basin when the snowpacks are extremely thin (< 20 mm). The majority of the peak SWE differences in the northern domain are due to differences between the satellite SWE estimates and the SNODAS simulation; the satellite products and GlobSnow-2 differences are limited to the northwestern part of the basin. The satellite peak SWE estimates in the forecast subbasins in the northern region are on average 40–125% larger than SNODAS with large differences in the center part of the basin near Grand Forks. Examination of concurrent records of ground and airborne observations from the region suggests that the low SWE may be due to lack of ground observations to update the SNODAS simulation. In contrast, the southern RRB shows no statistically significant differences in peak SWE among the products. In this region there is better radar coverage and a notably larger concentration of ground observations to inform the model simulations.

A strong agreement in peak SWE between the satellite and model estimates in the southern RRB increases confidence in both model and satellite SWE estimates. Moreover, it highlights the importance of satellite passive microwave SWE as an independent source for monitoring the seasonal snowpack and supporting improved snowmelt flood forecasts in regions where *in-situ* SWE observations may be limited and/or radar coverage is poor.

In summary, this paper documents that operational SWE observations from spaceborne passive microwave instruments differ from operationally derived model SWE simulations in data sparse regions such as the northern RRB. Based on these findings, this paper recommends that satellite SWE observations should be considered for improving operational snowmelt forecasting in the RRB. These improvements could be realized by considering satellite SWE observations as an independent source of information in the RRB for both the operational snowmelt forecast and SNODAS. Further support for this recommendation would benefit from comparison against *in-situ* observations and/or field campaigns. The authors further recommend preferred use of the SSM/I over the AMSR-E/2 product due to the demonstrated improved temporal performance relative to the model simulations.

REFERENCES

[1] P. E. Todhunter, "A hydroclimatological analysis of the red river of the north snowmelt flood catastrophe of 1997," *J. Amer. Water Resour. Assoc.*, vol. 37, no. 5, pp. 1263–1278, 2001.

[2] T. Carroll, *Airborne Gamma Radiation Snow Survey Program: A User's Guide*, version 5, 2001. [Online]. Available: https://www.nohrsc.noaa.gov/special/tom/gamma50.pdf, Accessed: Mar. 15, 2019.

[3] A. Carroll, T. Cline, D. Fall, G. Nilsson, A. Li, and L. Rost, "NOHRSC operations and the simulation of snow cover properties for the coterminous U.S.," in *Proc. 69th Annu. Meeting Western Snow Conf.*, 2001, pp. 1–14.

[4] R. a. Pielke, "Who decides? Forecasts and responsibilities in the 1997 red river flood," *Appl. Behav. Sci. Rev.*, vol. 7, no. 2, pp. 83–101, Jan. 1999.

[5] S. E. Tuttle, J. M. Jacobs, C. M. Vuyovich, C. Olheiser, and E. Cho, "Intercomparison of snow water equivalent observations in the northern great plains," *Hydrol. Process.*, vol. 32, no. 6, pp. 817–829, 2018.

[6] S. E. Tuttle *et al.*, *Remote Sensing of Hydrological Extremes*. Cham, Switzerland: Springer, 2017.

[7] National Operational Hydrologic Remote Sensing Center, *Snow Data Assimilation System (SNODAS) Data Products at NSIDC Version 1*. Boulder, CO, USA: National Snow and Ice Data Center, 2004. Accessed: Mar. 15, 2019. [Online]. Available: https://nsidc.org/data/g02158

[8] C. Vuyovich and J. M. Jacobs, "Snowpack and runoff generation using AMSR-E passive microwave observations in the Upper Helmand Watershed, Afghanistan," *Remote Sens. Environ.*, vol. 115, no. 12, pp. 3313–3321, Dec. 2011.

[9] C. M. Vuyovich, J. M. Jacobs, and S. F. Daly, "Comparison of passive microwave and modeled estimates of total watershed SWE in the continental United States," *Water Resour. Res.*, vol. 50, no. 11, pp. 9088–9102, Nov. 2014.

[10] D. Chen and H. W. Chen, "Using the Köppen classification to quantify climate variation and change: An example for 1901–2010," *Environ. Develop.*, vol. 6, no. 1, pp. 69–79, Apr. 2013.

[11] A. Walker and B. Goodison, "Discrimination of a wet snow cover using passive microwave datellite data," *Ann. Glaciol.*, vol. 17, pp. 307–311, 1993.

[12] M. Tedesco, R. Kelly, J. L. Foster, and A. T. Chang, *AMSR-E/Aqua Daily L3 Global Snow Water Equivalent Ease-Grids, Version 2*. Boulder, CO, USA: NASA National Snow and Ice Data Center Distributed Active Archive Center, 2004. Accessed: Jul. 15, 2017. [Online]. Available: http://dx.doi.org/10.5067/AMSR-E/AE_DYSNO.002

[13] P. Ashcroft and F. J. Wentz, *"AMSR-E/Aqua L2A Global Swath Spatially-Resampled Brightness Temperatures, Version 3*. Boulder, CO, USA: NASA National Snow and Ice Data Center Distributed Active Archive Center. 2013. Accessed: Jul. 15, 2017. [Online]. Available: http://dx.doi.org/10.5067/AMSR-E/AE_L2A.003

[14] R. Kelly, "The AMSR-E snow depth algorithm: Description and initial results," *J. Remote Sens. Soc. Jpn.*, vol. 29, no. 1, pp. 307–317, 2009.

[15] M. Tedesco, "Algorithm theoretical basis document snow algorithm." City University of New York, New York, NY, USA, Tech. Rep., 2012. [Online]. Available: http://nsidc.org/sites/nsidc.org/files/technical-references/amsr-atbd-supp12-snow.pdf

This article has been accepted for inclusion in a future issue of this journal. Content is final as presented, with the exception of pagination.

[16] A. Chang, J. Foster, and D. Hall, "Nimbus-7 SMMR derived global snow cover parameters," *Ann. Glaciol*, vol. 9, pp. 39–44, 1987.

[17] R. D. Brown and R. O. Braaten, "Spatial and temporal variability of Canadian monthly snow depths, 1946–1995," *Atmos.-Ocean*, vol. 36, no. 1, pp. 37–54, Mar. 1998.

[18] A. Krenke, *Former Soviet Union Hydrological Snow Surveys*. Boulder, CO, USA: National Snow and Ice Data Center, 2004. [Online]. Available: http://dx.doi.org/10.7265/N58C9T60

[19] M. Sturm, J. Holmgren, and G. E. Liston, "A seasonal snow cover classification system for local to global applications," *J. Clim.*, vol. 8, no. 5, pp. 1261–1283, May 1995.

[20] M. Sturm, B. Taras, G. E. Liston, C. Derksen, T. Jonas, and J. Lea, "Estimating snow water equivalent using snow depth data and climate classes," *J. Hydrometeorol.*, vol. 11, no. 6, pp. 1380–1394, 2010.

[21] R. L. Armstrong and M. J. Brodzik, "Recent northern hemisphere snow extent: A comparison of data derived from visible and microwave satellite sensors," *Geophys. Res. Lett.*, vol. 28, no. 19, pp. 3673–3676, Oct. 2001.

[22] J. Pulliainen, "Mapping of snow water equivalent and snow depth in boreal and sub-arctic zones by assimilating space-borne microwave radiometer data and ground-based observations," *Remote Sens. Environ.*, vol. 101, no. 2, pp. 257–269, 2006.

[23] M. Takala *et al.*, "Estimating northern hemisphere snow water equivalent for climate research through assimilation of space-borne radiometer data and ground-based measurements," *Remote Sens. Environ.*, vol. 115, no. 12, pp. 3517–3529, Dec. 2011.

[24] K. P. Luojus, J. T. Pulliainen, M. Takala, and T. K. M.Smolander, *Globsnow-2 Product User Guide*, version 1.0, 2013. [Online]. Available: www.globsnow.info/swe/GlobSnow2_SE_SWE_Product_User_Guide_v1_r1.pdf, Accessed: Mar. 15, 2019.

[25] J. T. Pulliainen, J. Grandell, and M. T. Hallikainen, "HUT snow emission model and its applicability to snow water equivalent retrieval," *IEEE Trans. Geosci. Remote Sens.*, vol. 37, no. 3, pp. 1378–1390, May 1999.

[26] J. Lemmetyinen *et al.*, "A comparison of airborne microwave brightness temperatures and snowpack properties across the boreal forests of Finland and Western Canada," *IEEE Trans. Geosci. Remote Sens.*, vol. 47, no. 3, pp. 965–978, Mar. 2009.

[27] M. Takala, J. Pulliainen, S. J. Metsamaki, and J. T. Koskinen, "Detection of snowmelt using spaceborne microwave radiometer data in Eurasia from 1979 to 2007," *IEEE Trans. Geosci. Remote Sens.*, vol. 47, no. 9, pp. 2996–3007, Sep. 2009.

[28] T. D. Carroll *et al.*, "NOAA's national snow analysis," in *Proc. Western Snow Conf.*, 2006, pp. 1–14.

[29] P. A. Miller and S. G. Benjamin, "A system for the hourly assimilation of surface observations in mountainous and flat terrain," *Monthly Weather Rev.*, vol. 120, no. 10, pp. 2342–2359, Oct. 1992.

[30] D. G. Tarboton and C. H. Luce, "Utah energy balance snow accumulation and melt model (UEB)," Utah Water Research Laboratory, Logan, UT, USA, 1996. [Online]. Available: https://www.fs.fed.us/rm/boise/publications/watershed/rmrs_1996_tarbotond001.pdf, Accessed: Mar. 15, 2019.

[31] R. E. Jordan, "User's Guide for USACRREL One-Dimensional Snow Temperature Model (SNTHERM.89)," U.S. Army Corps of Engineers, Hanover, NH, USA, Spec. Rep. 91-16, 1990.

[32] M. Hollander and D. Wolfe, *Nonparametric Statistical Methods*. Hoboken, NJ, USA: Wiley, 1973.

[33] O. J. Dunn, "Multiple comparisons using rank sums," *Technometrics*, vol. 6, no. 3, pp. 241–252, 1964.

[34] O. J. Dunn, "Multiple comparisons among means," *J. Amer. Stat. Assoc.*, vol. 56, no. 293, pp. 52–64, 1961.

[35] C. B. Young and N. A. Brunsell, "Evaluating NEXRAD estimates for the missouri river basin: Analysis using daily raingauge data," *J. Hydrol. Eng.*, vol. 13, no. 7, pp. 549–553, Jul. 2008.

[36] E. G. Josberger, N. M. Mognard, B. Lind, R. Matthews, and T. Carroll, "Snowpack water-equivalent estimates from satellite and aircraft remote-sensing measurements of the Red River basin, north-central U.S.A.," *Ann. Glaciol.*, vol. 26, no. 1982, pp. 119–124, Jan. 1998.

[37] M. Tedesco and P. S. Narvekar, "Assessment of the NASA AMSR-E SWE Product," *IEEE J. Sel. Top. Appl. Earth Obs. Remote Sens.*, vol. 3, no. 1, pp. 141–159, Mar. 2010.

[38] E. Cho, S. E. Tuttle, and J. M. Jacobs, "Evaluating consistency of snow water equivalent retrievals from passive microwave sensors over the north central U. S.: SSM/I vs. SSMIS and AMSR-E vs. AMSR2," *Remote Sens.*, vol. 9, no. 12, May 2017, Art. no. 465.

[39] A. T. C. Chang, J. L. Foster, and D. K. Hall, "Effects of forest on the snow parameters derived from microwave measurements during the boreas winter field compaign," *Hydrol. Process.*, vol. 10, no. 12, pp. 1565–1574, Dec. 1996.

[40] D. H. Kang, A. P. Barros, and S. J. Déry, "Evaluating passive microwave radiometry for the dynamical transition from dry to wet snowpacks," *IEEE Trans. Geosci. Remote Sens.*, vol. 52, no. 1, pp. 3–15, Jan. 2014.

[41] J. R. Wang and M. Tedesco, "Identification of atmospheric influences on the estimation of snow water equivalent from AMSR-E measurements," *Remote Sens. Environ.*, vol. 111, no. 2/3, pp. 398–408, Nov. 2007.

[42] M. Tedesco and J. R. Wang, "Atmospheric correction of AMSR-E brightness temperatures for dry snow cover mapping," *IEEE Geosci. Remote Sens. Lett.*, vol. 3, no. 3, pp. 320–324, Jul. 2006.

[43] T. Markus, D. C. Powell, and J. R. Wang, "Sensitivity of passive microwave snow depth retrievals to weather effects and snow evolution," *IEEE Trans. Geosci. Remote Sens.*, vol. 44, no. 1, pp. 68–77, Jan. 2006.

[44] E. G. Njoku, "Retrieval of land surface parameters using passive microwave measurements at 6–18 GHz," *IEEE Trans. Geosci. Remote Sens.*, vol. 37, no. 1, pp. 79–93, Jan. 1999.

[45] E. Njoku, T. Jackson, V. Lakshmi, T. K. Chan, and S. V. Nghiem, "Soil moisture retrieval from AMSR-E," *IEEE Trans. Geosci. Remote Sens.*, vol. 41, no. 2, pp. 215–229, Feb. 2003.

[46] R. Schroeder *et al.*, "Development and evaluation of a multi-year fractional surface water dataset derived from active/passive microwave remote sensing data," *Remote Sens.*, vol. 7, no. 12, pp. 16688–16732, Dec. 2015.

[47] M. Hallikainen, M. Vaaja, J. Seppanen, A. Hakkarainen, and J. Kainulainen, "Brightness temperature behavior of snow on lake ice over a wide frequency range," in *Proc. Int. Geosci. Remote Sens. Symp.*, 2014, pp. 2411–2414.

[48] A. Rees, J. Lemmetyinen, C. Derksen, J. Pulliainen, and M. English, "Observed and modelled effects of ice lens formation on passive microwave brightness temperatures over snow covered tundra," *Remote Sens. Environ.*, vol. 114, no. 1, pp. 116–126, Jan. 2010.

Ronny Schroeder received the B.Sc. degree in geography from Friedrich Schiller University, Jena, Germany, the M.Sc. degree in geography with emphasis in climatology and remote sensing from the same university and the Max Planck Institute for Biogeochemistry, Jena, Germany, and the Dr. rer. nat. degree from the University of Hohenheim, Stuttgart, Germany, in 2000, 2004, and 2016, respectively.

He was a Postdoctoral Scientist with the University of New Hampshire, Durham, New Hampshire, a Visiting Independent Advisor, and a Research Associate with Jet Propulsion Laboratory, California Institute of Technology, Pasadena, CA, USA, and Environmental CrossRoads Initiative, CREST Institute, City College of New York, City University of New York, New York, NY, USA. His research interest includes synergy of passive and active microwave remote sensing data to monitor Earth's water and carbon cycles. Recently his focus has shifted toward transforming research to real-world operations that directly benefit society.

Dr. Schroeder has been a member of the American Geophysical Union since 2007.

Jennifer M. Jacobs received the B. Sc. degree from Brown University, Providence, RI, USA; the M.S. degree from Tufts University, Medford, MA, USA, and the Ph.D. degree from Cornell University, Ithaca, NY, USA, in 1987, 1993, and 1997, respectively.

She is a Professor with the Department of Civil and Environmental Engineering with the University of New Hampshire, Durham, New Hampshire. She has over 25 years of experience using novel weather and climate information to enhance infrastructure design and practice with a specialty in cold weather and snow. She has authored and coauthored over 80 published journal articles on these topics. She is the Director of the National Science Foundation funded Research Coordination Network: The Infrastructure and Climate Network (ICNet). Her research interests include design and managing transportation infrastructure under a changing climate to numerous national and international organizations.

Dr. Jacobs was the Lead Author for the Transportation Sector Chapter of the 4th National Climate Assessment. She is the Hydrology Section Editor of *Remote Sensing in Earth Systems Science*.

Eunsang Cho received the B.S. and M.S. degrees in civil and environmental engineering from Hanyang University, Seoul, South Korea, in 2010 and 2014, respectively. He is currently working toward the Ph.D. degree in civil and environmental engineering with Earth Systems Research Center, Institute for the Study of Earth, Oceans, and Space (EOS) at University of New Hampshire, Durham, NH, USA.

His research interests include monitoring soil moisture, freeze/thaw, and snowpack from airborne and satellite remote sensing and its application to hydrological model. He is also interested in identifying human-induced landscape change (e.g., subsurface drainage system) using machine learning techniques and quantifying its impact on hydrological responses.

Carrie M. Olheiser received the B.S. degree in atmospheric sciences from the University of North Dakota, Grand Forks, ND, USA, in 1999.

From 1999 to 2002 she was a Graduate Research Assistant at University of North Dakota focusing on snow hydrology. Since 2002, she has been an Associate Scientist IV for the University Corporation for Atmospheric Research (UCAR); working at the National Weather Service National Operational Hydrologic Remote Sensing Center, Office of Water Prediction, Chanhassen, MN, USA. Her research interests include operational snow modeling and data assimilation, airborne gamma snow water equivalent, and soil moisture observations.

Michael M. DeWeese was born in Valley Center, Kansas, USA in 1958. He received the B.S. degree in watershed science from Colorado State University, Fort Collins, CO, USA, in 1987.

From 1987 to 1990, he was a Reclamation Hydrologist for the Utah Department of Natural Resources specializing in coal mining reclamation. In 1990, he joined US National Weather Service (NWS) as a Hydrologic Forecaster. From 1995 to 2018, he was with the NWS North Central River Forecast Center in Chanhassen, MN, USA, first as a Senior Hydrologist, then as the Development and Operations Hydrologist in charge of supervising hydrologic development activities and daily forecast operations. He has authored numerous journal articles and coauthored a chapter on river forecasting in *The Handbook of Applied Hydrology* (McGraw-Hill Education, 2017).

Mr. DeWeese was the recipient of both regional and national awards including the US Department of Commerce Gold Medal Award. He is a member of the American Geophysical Union.

Brian A. Connelly was born in St. Paul, MN, USA in 1966. He received the B.S. degree in physics from the University of Minnesota, Minneapolis, MN, USA, in 1990, and the M.S. degree in forest hydrology from the University of Washington, Seattle, WA, USA, in 1992.

From 1992 to 1993, he was a Research Assistant with the College of Forest Resources at the University of Washington helping develop a distributed hydrologic model. Since 1994, he has worked with National Weather Service North Central River Forecast Center, Chanhassen, MN, USA, as a Hydrologic Forecaster. His research interests include river ice processes, reservoir modeling, model calibration, programming, and cold region hydrology.

Michael H. Cosh (M'02–SM'17) received the Ph.D. degree in civil and environmental engineering from Cornell University, Ithaca, NY, USA, in 2002.

He is a Research Hydrologist with the U.S. Department of Agriculture, Agricultural Research Service, Hydrology and Remote Sensing Laboratory, Beltsville, MD, USA. His current research interests include the monitoring of soil moisture from both *in situ* resources and satellite products.

Xinhua Jia was born in Urumqi, Xinjiang, China. She received the B.S. degree in agronomy from Xinjiang Agricultural University, Urumqi, China, in 1987, and the M.S. and Ph.D. degrees in agricultural and biosystems engineering from University of Arizona, Tucson, AZ, USA in 2000 and 2004, respectively.

She is currently an Associate Professor with North Dakota State University (NDSU), Fargo, ND, USA. From 1987 to 1998, she worked as a Research Scientist with the Xinjiang Academy of Agricultural Sciences in Urumqi, Xinjiang, China. From 1998 to 2004, she worked as a Research and Teaching Assistant with the University of Arizona. From 2004 to 2007, she worked as a Postdoctoral Research Associate with the University of Florida, Gainesville, FL, USA. From 2007 to 2019, she was an Assistant/Associate Professor with the Department of Agricultural and Biosystems Engineering at NDSU. Her research interests include drainage water management, snow hydrology, water quality, and plastic mulch for high value crops.

Dr. Jia is a Professional Engineer with North Dakota State University (NDSU). She has been a member of ASABE, SSSA, and ASEE.

Carrie M. Vuyovich received the Ph.D. degree in civil engineering from the University of New Hampshire, Durham, NH, USA, in 2016.

She is a Research Physical Scientist at NASA Goddard Space Flight Center with Hydrological Sciences Laboratory, Greenbelt, MD, USA. Her current research includes study of seasonal, terrestrial snow to understand its impact on Earth's hydrological and land–atmosphere interaction processes, and evaluating remote sensing and modeling techniques to improve estimates of snowpack water supply and snowmelt runoff magnitude and timing.

Samuel E. Tuttle received the B.A. degree in geosciences from Williams College, Williamstown, MA, USA, in 2007, the M.A. degree in earth sciences and the Ph.D. degree in earth and environment from Boston University, Boston, MA, USA, in 2011 and 2015, respectively.

From 2015–2016, he was a Postdoctoral Scientist with the Department of Civil and Environmental Engineering, University of New Hampshire, Durham, NH, USA. Since 2017, he has been a Visiting Assistant Professor of data science with the Department of Geology and Geography, Mount Holyoke College, South Hadley, MA, USA. His research interests include characterizing relationships within the hydrological cycle, links between hydrology and climate, land-atmosphere interactions, and remote sensing of soil moisture, snow, and ice.

Dr. Tuttle was the recipient of the Outstanding Student Paper Award for the Hydrology section at the 2013 AGU Fall Meeting. He has been a member of American Geophysical Union since 2010.